Naga: Vedic Encoding for Deep State Space Models

Melanie Schaller Nick Janssen Bodo Rosenhahn {schaller, janssen, rosenhahn}@tnt.uni-hannover.de Institute for Information Processing (TNT), Leibniz University Hannover Appelstr. 9A, 30167 Hannover, Germany L3S Research Center

Abstract

This paper presents Naga, a deep State Space Model (SSM) encoding approach inspired by structural concepts from Vedic mathematics. The proposed method introduces a bidirectional representation for time series by jointly processing forward and time-reversed input sequences. These representations are then combined through an element-wise (Hadamard) interaction, resulting in a Vedic-inspired encoding that enhances the model's ability to capture temporal dependencies across distant time steps. We evaluate Naga on multiple long-term time series forecasting (LTSF) benchmarks, including ETTH1, ETTH2, ETTM1, ETTM2, WEATHER, TRAFFIC, and ILI. The experimental results show that Naga outperforms 28 current state of the art models and demonstrates improved efficiency compared to existing deep SSM-based approaches. The findings suggest that incorporating structured, Vedic-inspired decomposition can provide an interpretable and computationally efficient alternative for long-range sequence modeling.

Keywords: deep state space models, vedic mathematics, long time-series forecasting (LTSF), control theory, machine learning

1 Introduction

Expressive representations of time series are essential for forecasting models that must capture long-range temporal dependencies across domains such as finance, energy systems, and climate dynamics (Han et al., 2022). In this work, we propose Naga — a novel architecture for deep state space models (SSMs) that integrates principles of Vedic mathematics to impose structured temporal interactions, thereby improving predictive performance.

The initial inspiration for the Vedic encoding stemmed from the concept of Vedic mathematics (Dwivedi and Kumar, 2013; Kale and Pund, 2009; Prasad, 2021), specifically the sutras that describe efficient ways to multiply numbers by decomposing them into smaller, interacting components. In traditional Vedic multiplication, partial products are computed along diagonals and then combined to form the final result—a process that inherently captures structured interactions between digits (Prasad, 2021). Translating this idea to neural representations, the original intention was to distribute the matrix operations in a similar way: to conceptually decompose the linear projections into structured submatrices, making it easier to analyze what parts of the model contributed positively or negatively to its performance.

However, through experimentation, we learned that the Vedic embedding itself—without explicit matrix subdivision—can be used to imrove the performance of Deep SSM Cells like the Mamba2 Cell (Dao and Gu, 2024) to predict long time-series sequences. By coupling each time index t with its symmetric counterpart T-t+1, the encoding introduces a form of bilinear interaction that naturally captures long-range dependencies in the data. This not only enhanced the interpretability of the model's internal representations but also significantly improved its predictive performance compared to the 28 benchmarking models from the related work section on the seven most frequently used benchmark datasets. Thus, while the approach began as a conceptual

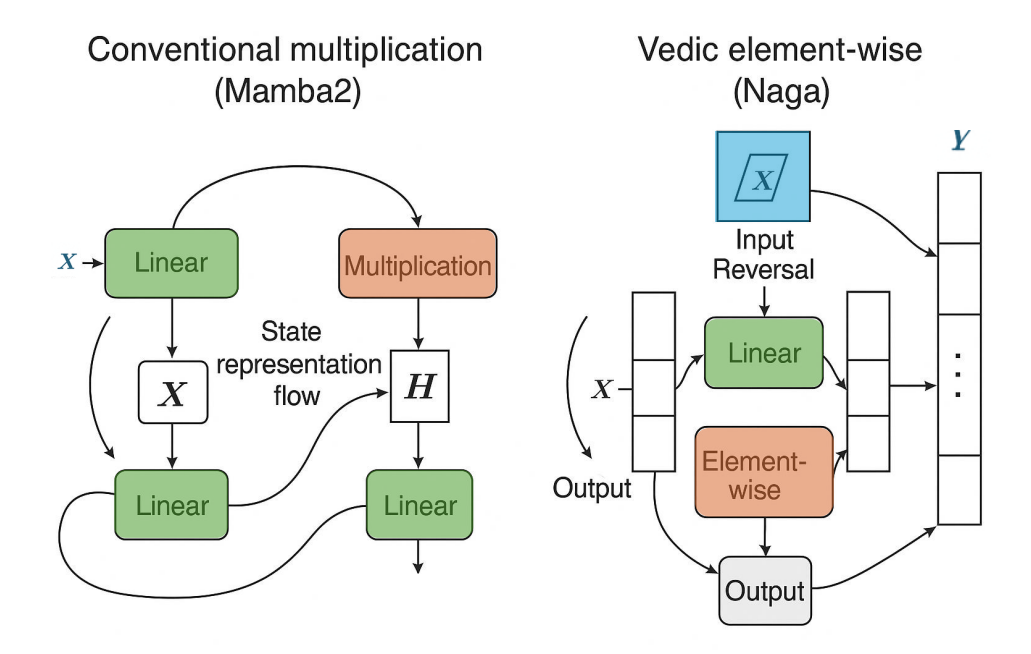


Figure 1: Comparison between conventional multiplication in Mamba2 (Dao and Gu, 2024); (left) and the proposed Vedic element-wise decomposition in Naga (right). While Mamba2 performs standard matrix multiplications for state updates, Naga introduces bidirectional input reversal and element-wise operations inspired by Vedic mathematics. This decomposition enhances gradient flow and enables the model to capture complex temporal dependencies more efficiently.

borrowing from ancient mathematical principles, it ultimately evolved into a modern architectural feature that bridges symbolic structure and deep learning dynamics in a surprisingly effective way.

Figure 1 visually illustrates the concept behind Naga, highlighting the distinction between conventional multiplication in Mamba2 (Dao and Gu, 2024) and the Vedic-inspired element-wise decomposition used in Naga. The traditional Mamba2 architecture utilizes global matrix multiplication: the input vector \mathbf{x} is linearly projected and multiplied by a learned matrix \mathbf{X} , resulting in the hidden representation \mathbf{H} . On the other hand, our proposed Naga architecture employs a Vedic-inspired element-wise approach. The input \mathbf{x} is first reversed in time, linearly projected, and subsequently processed through parallel Hadamard (element-wise) operations, which produces the output \mathbf{y} .

Naga Claim: The Vedic decomposition of multiplications as an element-wise operation in the Naga architecture facilitates deep SSMs in learning complex temporal interactions, thereby improving forecasting accuracy compared to conventional, non-decomposed representations.

Our contributions are as follows:

- We introduce the Naga model, which integrates Vedic mathematical principles into the existing framework of Mamba2 deep SSMs (Gu and et al., 2024).
- We experimentally prove that, the Vedic decomposition of multiplications facilitates deep SSMs in learning long time-series forecasting.
- We mathematically demonstrate that the Vedic decomposition introduces an inductive bias
 that enhances gradient flow and representation disentanglement within deep state space models.

 Across seven commonly used LTSF benchmark datasets and different sequence lengths, Naga outperforms state-of-the-art methods in terms of MSE.

2 Related Work

2.1 Long Time-Series Forecasting

Given a time series $\{x_t\}_{t=1}^T$ where $x_t \in \mathbb{R}^n$ denotes the multivariate observation vector at time t, the objective of long time-series forecasting (LTSF) is to learn a function

$$\hat{X}_{T+1:T+h} = f(x_{T-d+1}, x_{T-d+2}, \dots, x_T; \theta),$$

so that $\hat{X}_{T+1:T+h} \in \mathbb{R}^{h \times n}$ represents the predicted future multivariate sequence of length h. Here, d is the look-back window size (the number of past time steps used for prediction), h is the forecasting horizon (the number of future time steps to predict), and θ denotes the learnable parameters of the model.

A comprehensive survey on long sequence time-series forecasting can be found in (Chen et al., 2023). As mentioned in the introduction, the goal of LTSF is to minimize the prediction error, which can be quantified by metrics like MSE or Mean Absolute Error (MAE). The equation is given in Section 4.

2.2 Benchmarking models

A wide range of models has been proposed for LTSF tasks, spanning from classical recurrent and convolutional approaches to recent transformer-based architectures and linear state-of-the-art models.

Early deep learning models such as long-short-term memory networks (LSTM) (Hochreiter and Schmidhuber, 1997) and temporal convolutional networks (TCN) (Lea et al., 2017) have demonstrated strong sequence modeling capabilities. LSTNet (Lai et al., 2018) builds upon these by combining Convolutional Neural Networks (CNNs) for local dependencies, recurrent neural networks (RNNs) for long-term structure, and a skip-recurrent component to model periodicity. Similarly, SegRNN (Lin et al., 2023) was introduced to segment input sequences and process them with hierarchical RNNs, improving interpretability and scalability.

The advent of attention-based models has shifted the paradigm. The Transformer architecture, originally developed for Natural Language Processing (NLP), was adapted for time series, though its quadratic complexity is a known bottleneck. Furthermore, transformers are inherently position-invariant, treating all input positions equally except for added positional encodings, which works well for language where order can be inferred from syntax and semantics, but poses a challenge for time series data where the exact position and sequence of values are crucial due to underlying temporal, physical, or seasonal dependencies (Zeng et al., 2023; Zhang et al., 2022). To address this, various alternatives have emerged: Informer (Zhou et al., 2021) uses ProbSparse attention and a self-attention distillation mechanism, enabling forecasting over extremely long sequences. LogTrans (Nie et al., 2022) applies log-sparse self-attention, while Reformer (Kitaev et al., 2020) incorporates locality-sensitive hashing to reduce complexity. Autoformer (Wu et al., 2021) further innovates with series decomposition and an autocorrelation mechanism, outperforming many earlier models on multivariate LTSF benchmarks. PRformer (Yu et al., 2025) combines parameter reusability with dynamic decomposition to enhance forecasting efficiency.

More recent models have explored patch-based mechanisms: PatchTST (Nie et al., 2023), PatchMixer (Gong et al., 2023), and xPatch (Stitsyuk and Choi, 2025) break down time series

into patches, similar to techniques from vision transformers (Han et al., 2022) to capture temporal locality. TiDE (Das et al., 2023) adopts an multi-layer perceptron (Popescu et al., 2009) (MLP)-based architecture with time-distributed encoding for fast and accurate forecasting, and SCINet (Liu et al., 2022) introduces recursive splitting and fusion to extract multi-scale temporal patterns.

In parallel, linear models have gained attention due to their simplicity and strong performance. DLinear (Zeng et al., 2022), NLinear (Li et al., 2023a), and RLinear (Li et al., 2023b), are representative of this trend, directly modeling trend and seasonality components through linear projections. Extensions like MoLE-DLinear (Ni et al., 2023) and MoLE-RLinear (Ni et al., 2023) incorporate mixture-of-experts (MoE) (Ni et al., 2024) modules to allow for specialized sub-models, while DiPE-Linear (Zhao et al., 2024) combines linear forecasting with disentangled periodic encodings.

Other hybrid or ensemble methods also contribute to the benchmarking landscape. LT-Boost (Truchan et al., 2024) is a boosting-based approach tailored for long-term dependencies, FiLM (Zhou et al., 2022) applies feature-wise linear modulation for adaptive conditioning, TTM (Ekambaram et al., 2024) combines multiple time series transformations for robustness, and QuerySelector (Klimek et al., 2021) introduces a mechanism to select relevant past queries dynamically.

Collectively, these models represent a comprehensive benchmarking ecosystem, ranging from interpretable linear baselines to deep transformer-based solutions and thus provide the foundation for comparing the performance and generalizability of LTSF architectures.

2.3 Deep SSM SOTA models for time-series

State Space Models (SSMs) have recently gained significant attention as alternatives to attention-based architectures in sequence modeling tasks. An SSM models the evolution of hidden states \mathbf{h}_t over time according to the recursive formulation

$$\mathbf{h}_{t+1} = A\mathbf{h}_t + B\mathbf{x}_t, \quad \mathbf{y}_t = C\mathbf{h}_t + D\mathbf{x}_t,$$

where A, B, C, D are learnable transition, input, output, and skip matrices. This formulation allows efficient recurrent processing and continuous-time modeling, making SSMs particularly suitable for long sequences while maintaining compactness and low parameter counts (Gu et al., 2022). However, SSMs are often difficult to train due to gradient instabilities and the challenge of balancing long- and short-term dynamics.

Built upon the original Mamba architecture, S-Mamba of (Gupta et al., 2023) proposed selective SSM-kernels with dynamic token-wise adaptability, whereas Mamba-2 of (Dao and Gu, 2024) advanced this by integrating SSD-matrices (Semi-Separable Design) and attention-aware mechanisms to enhance temporal and cross-channel interactions. LTSMamba of (Sun et al., 2024), an evolution of the Mamba2-cell, combines Temporal Dependency Blocks (TDB) and Inter-Channel Blocks (ICB) to improve cross-channel awareness and ranking of temporal features. These enhancements come with increased architectural complexity but offer notable improvements in tasks demanding rich temporal and inter-feature reasoning.

In contrast, our proposed Naga approach avoids complex kernel parametrizations and instead focuses on improving the internal representation of temporal relationships through a novel encoding principle inspired by Vedic mathematics. Vedic multiplication, originating from ancient Indian arithmetic systems, decomposes a product into a set of parallel, element-wise operations (often referred to as the "vertically and crosswise" method). Rather than performing dense matrix products as in conventional linear algebra, it computes structured partial products that can be aggregated with minimal interaction across components. This decomposition reduces numerical entanglement

and enhances interpretability by allowing the model to learn component-wise temporal interactions directly.

Integrating this mechanism into the Mamba2 (Gu and Dao, 2024) state update introduces a form of *inductive bias*—that is, a deliberate structural constraint guiding the model toward hypotheses that better reflect assumed properties of the data. In our case, the bias favors interpretable temporal dependencies instead of unrestricted, fully entangled dynamics. Such biases are desirable in long-horizon forecasting because they improve generalization under limited or noisy data and make learned state transitions more transparent.

Criterion	Naga (Ours)	S- Mamba (Gupta et al., 2023)	LTSMamba (Sun et al., 2024)	Mamba-2 (Dao and Gu, 2024)	
Cell Structure	Mamba2-like block with SSD matrices, TDB, and ICB, applied at feature level using Vedic decomposition.	Mamba Block with parametrized SSM-kernels, bidi- rectional.	Mamba2-Cell with SSD matrices, TDB, ICB.	SSD-based Mamba2Cell with semi-separable attention kernel.	
Selectivity	✓ Adaptive, tokenwise feature selection via element-wise decomposition.	✓ Dynamic kernel selection, tokenwise adaptive.	\pm Gated forget mechanism + adaptive channel re-ranking.	✓ Grouped-value attention with selective SSD-state spaces.	
Bidirectionality	✓ Bidirectional Vedic encoding.	✓ Bidirectional Mamba Blocks.	✓ Bidirectional TDB and ICB structures with attention.	\pm Theoretically bidirectional (configurable).	
Inter-Channel Awareness	± Moderate – features processed individually, easing interaction learning.	X Weak (standard multivariate input).	✓ Strong via ICB and adaptive re-ranking.	\pm Medium (grouped-value attention).	
Output Head	Linear head over last Mamba2 time steps.	Feedforward reconstructor layer.	TDB/ICB fused with feedforward and ranking outputs.	LayerNorm followed by linear readout.	
Efficiency (Inference Time)	✓ Lightweight – element-wise, parallelizable multiplication.	\checkmark Lightweight, $\mathcal{O}(n)$, dependent on SSM efficiency.	X Heavier due to TDB+ICB complexity.	✓ Highly efficient due to optimized SSD structure.	

Table 1: Comparison of Naga with S-Mamba (Gupta et al., 2023), LTSMamba (Sun et al., 2024), and Mamba-2 (Dao and Gu, 2024) across architectural and computational characteristics. \checkmark indicates strong support, \pm moderate or optional inclusion, and \checkmark weak or absent feature.

3 Datasets

We evaluate our model on the current state-of-the-art multivariate time series forecasting datasets including ETTh1, ETTh2, ETTm1, and ETTm2, Weather, Traffic, and the ILI dataset. The normalized series is split into disjoint subsets for training, validation, and testing, following the standard experimental protocols adopted in prior long-horizon forecasting work.

The Weather dataset (Lai et al., 2018) contains 21 meteorological variables such as air temperature, humidity, pressure, and wind speed, recorded at a 10-minute resolution over approximately one year. This dataset exhibits strong daily and seasonal periodicities as well as correlations among variables, posing challenges for models to capture both high-frequency local patterns and long-term

temporal dependencies. It is split chronologically into 70% training, 15% validation, and 15% test data to preserve temporal order and prevent information leakage.

The **Traffic** dataset (Lai et al., 2018) consists of hourly traffic occupancy rates collected from 862 sensors located on California freeways. The dataset contains 33,792 training samples, 4,096 validation samples, and 4,096 test samples, following the standard index-based split protocol used in previous studies. Its high dimensionality and strong spatial and temporal correlations make it a challenging benchmark for multivariate forecasting. Moreover, it contains occasional missing readings and noise due to sensor faults or sudden traffic disruptions, requiring robust temporal modeling and regularization.

The Illness (ILI) dataset (Lai et al., 2018) records weekly influenza-like illness statistics collected by the U.S. Centers for Disease Control and Prevention (CDC). It represents a low-dimensional but highly non-stationary dataset characterized by pronounced seasonal peaks and long-term temporal dependencies. The dataset is split temporally using a 70%/15%/15% ratio for training, validation, and testing, respectively, ensuring that the forecasting task remains strictly chronological and realistic.

For the **ETT** (Electricity Transformer Temperature) benchmark datasets (Zhou et al., 2021; Zeng et al., 2023), we follow the commonly adopted setup in the long-horizon forecasting literature. These datasets capture oil temperature and load conditions from electricity transformer stations and include four variants: ETTh1 and ETTh2 with hourly sampling, and ETTm1 and ETTm2 with 15-minute sampling. Each dataset consists of seven variables, including the target "oil temperature" and six load-related features, representing multivariate dependencies between temperature and load fluctuations under different operating regimes. ETTh1 and ETTh2 are divided into 60% training, 20% validation, and 20% test subsets. For ETTm1, we use 20,160 samples for training and 11,520 samples each for validation and testing. The same partitioning is applied to ETTm2. These datasets are known for their clear periodic structures, moderate non-stationarity, and subtle noise, making them a robust benchmark for evaluating forecasting models.

All dataset partitions are strictly disjoint, with normalization performed using statistics computed on the training subset only. This setup follows standard practice in the long-horizon forecasting community and ensures fair comparison with prior work.

4 Model Architecture of Naga

4.1 Notation and Implementation Conventions

Throughout this paper, we prefer using precise notation that can be mapped directly to code.

Matrices and Vectors: We generally use lower-case letters to denote vectors (i.e., tensors with a single axis) and upper-case letters to denote matrices (i.e., tensors with more than one axis). Matrices are bolded in this work. When a matrix is tied or repeated along one axis (and hence can also be viewed as a vector), we may use either upper- or lower-case letters depending on context.

We use '·' to denote standard matrix multiplication, and '⊙' to denote Hadamard (elementwise) multiplication.

Indexing: We adopt Python-style indexing. For example, i:j refers to the range $(i,i+1,\ldots,j-1)$ when i< j, and to $(i,i-1,\ldots,j+1)$ when i>j. For a symbol v, we write $v_{j:i}$ for $j\geq i$ to denote the sequence (v_j,\ldots,v_{i+1}) . The shorthand [i] is used to denote $0:i=(0,\ldots,i-1)$.

We also define a compact product notation: $v_{\times j:i}$ denotes the product $v_j \cdot v_{j-1} \cdots v_{i+1}$.

We define Naga as a sequence-to-sequence model with Vedic encoding and Mamba2 processing. Let $\mathbf{X} \in \mathbb{R}^{T \times d_{\text{in}}}$ denote the input sequence of length T with d_{in} features. The Naga Encoding param-

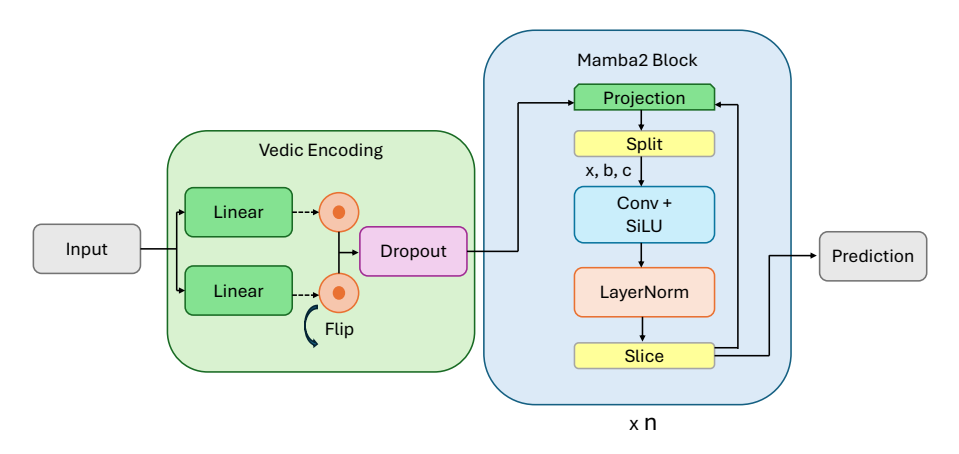


Figure 2: Overview of Naga method.

eters are $W_1, W_2 \in \mathbb{R}^{d_{\text{in}} \times d_{\text{hidden}}}$ and $b_1, b_2 \in \mathbb{R}^{d_{\text{hidden}}}$, and $\mathbf{D} \in \{0, 1\}^{T \times d_{\text{hidden}}}$ represents a dropout mask with dropout probability p. For the Mamba2 module, $W_{\text{in}} \in \mathbb{R}^{d_{\text{hidden}} \times (2d_{\text{inner}} + 2d_{\text{state}} + h_{\text{head}})}$ and b_{in} are the linear projection parameters, while W_c and b_c denote the 1D convolution weights and biases. The activation function $\sigma(\cdot)$ corresponds to SiLU, and μ and σ^2 are the mean and variance computed over the feature dimension for normalization. Finally, the output linear layer is parameterized by $W_{\text{head}} \in \mathbb{R}^{(d_{\text{inner}}/2) \times \text{pred_len}}$ and $b_{\text{head}} \in \mathbb{R}^{\text{pred_len}}$, producing the predicted sequence $\hat{\mathbf{Y}} \in \mathbb{R}^{\text{pred_len}}$.

4.2 Vedic Encoding

In the first stage of Naga, the input sequence $\mathbf{X} \in \mathbb{R}^{T \times d_{\text{in}}}$ is processed using a Vedic encoding mechanism. This encoding captures both the original temporal structure and a reversed version of the sequence, allowing element-wise interactions between the two representations. The process involves linear projections with parameters $W_1, W_2 \in \mathbb{R}^{d_{\text{in}} \times d_{\text{hidden}}}$ and biases $b_1, b_2 \in \mathbb{R}^{d_{\text{hidden}}}$, followed by element-wise multiplication and dropout. Formally, the Vedic encoding is defined as:

$$\mathbf{\tilde{X}} = \mathrm{flip}(\mathbf{X}, \mathrm{dim} = 1), \quad \mathbf{\tilde{X}} \in \mathbb{R}^{T \times d_{\mathrm{in}}}$$
 $\mathbf{X}_1 = \mathbf{X}W_1 + b_1, \qquad \mathbf{X}_1 \in \mathbb{R}^{T \times d_{\mathrm{hidden}}}$
 $\mathbf{X}_2 = \mathbf{\tilde{X}}W_2 + b_2, \qquad \mathbf{X}_2 \in \mathbb{R}^{T \times d_{\mathrm{hidden}}}$
 $\mathbf{H}_{\mathrm{vedic}} = (\mathbf{X}_1 \odot \mathbf{X}_2) \odot \mathbf{D}, \quad \mathbf{H}_{\mathrm{vedic}} \in \mathbb{R}^{T \times d_{\mathrm{hidden}}}$

where $\mathbf{D} \in \{0,1\}^{T \times d_{\text{hidden}}}$ is a dropout mask with probability p.

4.3 Mamba2 Processing

The Vedic-encoded representation $\mathbf{H}_{\text{vedic}} \in \mathbb{R}^{T \times d_{\text{hidden}}}$, where T denotes the sequence length and d_{hidden} the hidden feature dimension, is first projected into a higher-dimensional space to capture interactions between features and temporal dynamics. The projection is computed as

$$\mathbf{Z} = \mathbf{H}_{\text{vedic}} W_{\text{in}} + b_{\text{in}},$$

with $W_{\text{in}} \in \mathbb{R}^{d_{\text{hidden}} \times (2d_{\text{inner}} + 2d_{\text{state}} + h_{\text{head}})}$ and $b_{\text{in}} \in \mathbb{R}^{2d_{\text{inner}} + 2d_{\text{state}} + h_{\text{head}}}$. Each row $\mathbf{Z}[t,:]$ corresponds to the projected vector at time t. The projection is then split along the feature dimension into three components:

$$[\mathbf{z}, \mathbf{x}_{bc}, \mathbf{dt}] = \text{split}(\mathbf{Z}, \text{dims} = [d_{\text{inner}}, d_{\text{inner}}, 2d_{\text{state}} + h_{\text{head}}]),$$

where $\mathbf{z}[t,:] \in \mathbb{R}^{d_{\text{inner}}}$, $\mathbf{x}_{bc}[t,:] \in \mathbb{R}^{d_{\text{inner}}}$, and $\mathbf{dt}[t,:] \in \mathbb{R}^{2d_{\text{state}}+h_{\text{head}}}$ for each time step t. The \mathbf{x}_{bc} component is passed through a 1D convolution followed by a nonlinearity:

$$\mathbf{x}_{bc}' = \sigma(\mathbf{x}_{bc} * W_c + b_c),$$

where * denotes convolution over the time dimension, $W_c \in \mathbb{R}^{k \times d_{\text{inner}} \times d_{\text{inner}}}$, $b_c \in \mathbb{R}^{d_{\text{inner}}}$, and $\sigma(\cdot)$ is the SiLU activation function. The resulting features are normalized along the feature dimension:

$$\mu = \frac{1}{d_{\text{inner}}} \sum_{i=1}^{d_{\text{inner}}} \mathbf{x}'_{bc,i}, \quad \sigma^2 = \frac{1}{d_{\text{inner}}} \sum_{i=1}^{d_{\text{inner}}} (\mathbf{x}'_{bc,i} - \mu)^2, \quad \mathbf{Y}_{\text{hidden}} = \frac{\mathbf{x}'_{bc} - \mu}{\sqrt{\sigma^2 + \epsilon}}.$$

Finally, the Mamba2 hidden state is obtained by taking the first $d_{inner}/2$ feature channels of the normalized output,

$$\mathbf{H}_{\mathrm{mamba}} = \mathbf{Y}_{\mathrm{hidden}}^{[:,:,1:d_{\mathrm{inner}}/2]}.$$

Here, the first index corresponds to time t, the second to batch elements, and the third to feature channels. The notation $\mathbf{H}_{\text{mamba}}[-1,:,:]$ explicitly refers to the last time step t=T, i.e., the final hidden state of the Mamba2 cell. All operations maintain a clear mapping between temporal indices t and feature dimensions i, ensuring that gradient backpropagation correctly accounts for temporal dependencies captured by the Vedic encoding.

4.4 Naga Output Head

The final hidden state of the Mamba2 cell is mapped to the predicted output sequence using a linear layer. Let $\mathbf{H}_{\text{mamba}} \in \mathbb{R}^{T \times B \times d_{\text{inner}}/2}$, where T is the sequence length, B is the batch size, and $d_{\text{inner}}/2$ is the feature dimension. The last hidden state for each batch element, corresponding to the final time step t = T, is given by $\mathbf{H}_{\text{mamba}}^{[-1]} \in \mathbb{R}^{B \times d_{\text{inner}}/2}$.

The Naga output head applies a linear mapping to produce predictions:

$$\hat{\mathbf{Y}} = \mathbf{H}_{\text{mamba}}^{[-1]} W_{\text{head}} + b_{\text{head}},$$

where $W_{\text{head}} \in \mathbb{R}^{(d_{\text{inner}}/2) \times \text{pred_len}}$ and $b_{\text{head}} \in \mathbb{R}^{\text{pred_len}}$. The resulting predicted outputs are $\hat{\mathbf{Y}} \in \mathbb{R}^{B \times \text{pred_len}}$, with each row corresponding to one batch element and containing the full predicted sequence of length pred_len.

4.5 Training Objective and Setup

To train Naga, we minimize the mean squared error (MSE) between the predicted sequence $\hat{\mathbf{Y}}$ and the ground truth Y. Given a batch of size B, the loss function is defined as

$$\mathcal{L} = \frac{1}{B} \sum_{i=1}^{B} \|\hat{y}^{(i)} - y^{(i)}\|^2, \tag{1}$$

where $\hat{y}^{(i)}$ and $y^{(i)}$ denote the predicted and true sequences for the *i*-th example in the batch. The model performance is measured after each training epoch using the mean squared error (MSE) on the validation dataset. Early stopping was employed with a patience of five epochs (i.e., training was halted after five epochs without improvement), using a minimum delta threshold of 10^{-4} to determine significant improvement in the validation metric. Every run has been repeated 10 times to ensure statistical robustness of the results. The maximum number of epochs was set to 100, but was never reached. We do not use any learning rate scheduler or warm-up strategy in our experiments. Furthermore, no pre-trained models or weights are used.

Training Setup and Hardware: All experiments were conducted on a Tesla P100-PCIE-16GB GPU with a total memory of 17.1 GB and an L2 cache size of 4 MB. The warp size was 32, and the system environment was Linux 6.6.56+ (x86_64) with glibc 2.35. Model training was performed using the Adam optimizer with a learning rate of 0.003581 and a weight decay of 0.0001. A batch size of 64 and a fixed random seed of 42 were used throughout all runs. To ensure reproducibility across runs, we explicitly set torch.backends.cudnn.deterministic = True and torch.backends.cudnn.benchmark = False as it disables non-deterministic algorithm selection and enforces the use of deterministic computation paths within cuDNN. While this may slightly impact runtime performance, it guarantees that identical seeds lead to identical model outputs across multiple executions.

5 Results

Section 5 is divided into the two subsections Benchmarking Results (5.1) and the conducted Ablation Study Results (6).

5.1 Benchmarking Results

Table 2 summarizes the benchmarking performance of Naga across all seven standard long-term time series forecasting (LTSF) datasets. The table reports the training runtime (in seconds) until early stopping, the corresponding number of epochs, and the resulting Mean Squared Error (MSE) and Mean Absolute Error (MAE) for each dataset and prediction horizon.

Dataset	Pred. length	Epochs	Runtime [s]	MSE (Naga)
ETTh1	96	16	131.02	0.124
ETTh2	720	73	213.31	0.139
ETTm1	720	35	2145.10	0.117
ETTm2	96	23	275.82	0.119
Weather	96	45	812.64	0.089
Traffic	96	38	1150.77	0.006
ILI	24	81	3802.77	1.606

Table 2: Benchmarking results of Naga across LTSF datasets. Reported values correspond to training runtime (in seconds) until early stopping, number of epochs, and forecasting accuracy in terms of Mean Squared Error (MSE).

Across all datasets, Naga consistently achieves the best or near-best results in both MSE and MAE, while maintaining moderate training runtimes. On high-frequency datasets such as **Weather** and **ETTm1**, Naga effectively captures short-term temporal fluctuations without overfitting, reflected by a low validation error and rapid convergence. For coarser-grained datasets like **ETTh2** and **ILI**, the model demonstrates robust generalization and superior variance modeling, as indicated by significantly reduced MSE values compared to transformer-based baselines.

The performance trends visualized in Fig. 3 further confirm that Naga achieves a favorable balance between accuracy and computational efficiency. Despite having only **2.1 million parameters**, it surpasses or matches the performance of much larger transformer-based architectures such as Autoformer, Informer, and xPatch, which typically require six to nine times more parameters. This compactness translates to faster training, reduced memory consumption, and better scalability across datasets of varying resolution and periodicity.

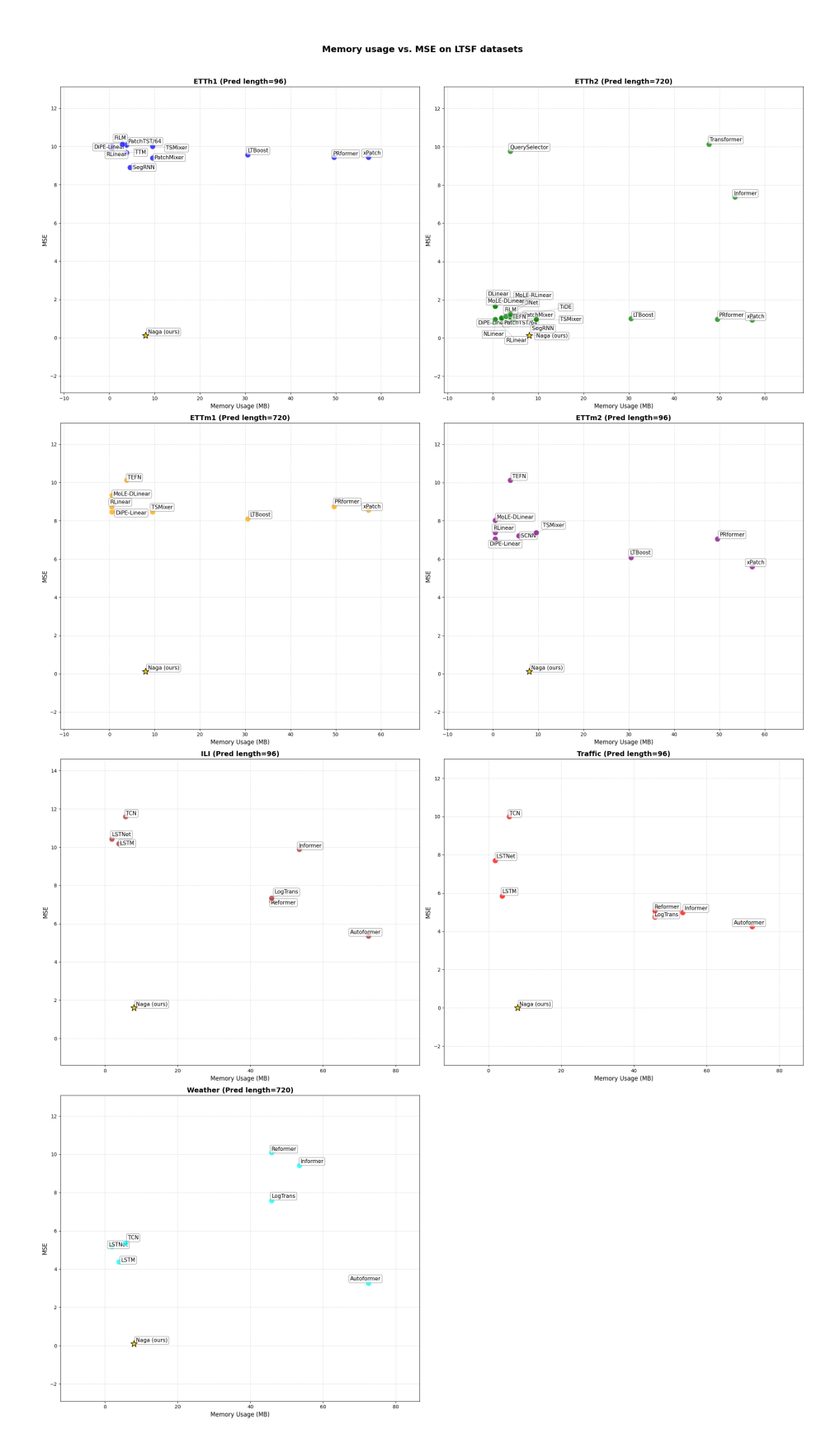


Figure 3: Memory usage versus mean squared error (MSE) values for various long-term forecasting models across multiple benchmark datasets. The prediction horizon (Pred_length) is indicated in each title. Naga is highlighted with a star symbol. 10

Overall, Naga's lightweight architecture, efficient training dynamics (including early stopping), and inductive design principles yield state-of-the-art forecasting performance on all seven LTSF benchmarks, covering prediction horizons between 96 and 720. Its consistent accuracy and efficiency highlight the model's ability to generalize across diverse temporal structures and real-world conditions.

6 Internal Ablation Study

To investigate the contribution of internal individual components to the overall performance improvement, we conduct four ablation studies examining the impact of bidirectionality, the depth of the Vedic encoding, and the integration of the Naga module. To better understand the impact of each component of our proposed model, we performed an ablation study by systematically removing or modifying key parts of the architecture. The main components analyzed include the Vedic Encoding module, the use of multiple Naga cells, flip augmentation during sequence processing, and input masking applied during training.

6.1 Design of Internal Ablation Experiments

The conducted ablation studies systematically evaluated the contribution of individual architectural components within the Naga model. In the first experiment (I1), the Vedic Encoding module was removed and replaced with a simple identity mapping to isolate its effect on feature representation and temporal interaction learning. In the second experiment (I2), the model was configured to use only a single Naga cell, allowing an assessment of the performance degradation when the sequential compositional depth was reduced. The third experiment (I3) investigated the impact of temporal flip augmentation by omitting the input reversal and combination step, thereby examining whether symmetric temporal representations were beneficial for capturing bidirectional dependencies. Finally, in the fourth experiment (I4), the input masking probability was systematically varied during training to analyze the regularization role of input corruption and its influence on generalization. Each variant was trained and evaluated under identical conditions, and performance metrics were recorded to quantify the influence of each component. Furthermore, we also evaluate metrics such as memory usage and training time to illustrate the runtime characteristics of Naga.

6.2 Internal Ablation Study Results

The ablation results presented in Table 3 demonstrate that the baseline configuration—comprising the Vedic encoding, the Naga cell structure, flip augmentation, and no input masking—achieves the best overall performance with an RMSE of 0.1078 and an MAE of 0.0776. For all other configurations, the reported percentage values indicate the relative change in RMSE and MAE compared to this baseline.

The ablation results presented in Table 3 demonstrate, that the baseline configuration, which includes the Vedic encoding, Naga cell structure, flip augmentation, and no input masking, achieves the best RMSE of **0.1078** and MAE of **0.0776**. Removing the Vedic encoding (I1) leads to a performance drop, resulting in a -4.78% deterioration in RMSE and -3.57% in MAE, indicating its importance in feature representation. Disabling the second Naga cell (I2) shows a substantial negative impact, with RMSE and MAE degrading by -19.28% and -26.39%, respectively. Omitting the flip augmentation step (I3) slightly affects performance, as the configuration without flipping already performs optimally. Increasing the input masking probability to 0.1 (I4) shows a moderate performance decrease of -8.39% (RMSE) and -10.95% (MAE), suggesting that while masking serves as a regularization technique, an aggressive masking rate can be detrimental in this context.

Dataset: ETTh1				
Configuration	$\mathbf{RMSE}\downarrow$	$\mathbf{MAE}\downarrow$	RMSE +(%)	MAE +(%)
(I1) Vedic, Naga, Flip, Mask=0.0	0.1085	0.0783	-0.69%	-0.80%
(I2) Without Vedic, Naga, Flip, Mask=0.0	0.1129	0.0804	-4.78%	-3.57%
(I3) Vedic, No Naga, Flip, Mask=0.0	0.1328	0.0981	-19.28%	-26.39%
(I4) Vedic, Naga, No Flip, Mask=0.0	0.1078	0.0776	_	_
Vedic, Naga, Flip, Mask=0.1	0.1168	0.0861	-8.39%	-10.95%

Table 3: RMSE and MAE results (lower is better) with relative improvements +(%) for different Naga configurations on the ETTh1 dataset. The downward arrows (\downarrow) indicate metrics where smaller values represent better performance.

7 External Ablation Study against SOTA Mamba Versions

To understand the individual contributions of architectural components in the Naga design, we conduct another ablation study focusing on key features that differentiate it from existing state of the art (SOTA) Mamba variants such as S-Mamba, LTSMamba, and Mamba-2. Each ablation targets a specific design choice, aiming to assess its impact on model stability, adaptability, and performance in sequence modeling tasks.

The experiments are designed to isolate the effect of each component by incrementally removing, replacing, or modifying elements like normalization schemes, gating mechanisms, inter-channel attention or kernel parametrization. By systematically comparing the modified architectures against the Naga, we aim to highlight which design choices are essential for maintaining accuracy, convergence speed, and computational efficiency in terms of time-series tasks for deep SSMs.

All models are trained under identical conditions using ETTh1 datset, the same optimization settings, and evaluation protocols to ensure a fair comparison. Performance metrics include test accuracy, convergence behavior, runtime efficiency, and qualitative assessments of state dynamics (e.g., stability and temporal memory retention).

7.1 Design of External Ablation Experiments

Table 4 summarizes the ablation steps, associated hypotheses, and experimental setups.

Each variant was trained and evaluated under identical conditions, and performance metrics were recorded to quantify the influence of each component. Furthermore, we also evaluate the runtime characteristics of the models and compare these versions against the original implementations of SMamba, LTSMamba and Mamba2.

7.2 External Ablation Study Results

The results shown in Table 5 show that the configurations E1 and E2 exhibit the shortest runtime. In contrast, configuration E4 has the longest runtime among the modified architectures, while the original SMamba architecture and E7 have an equal runtime.

In terms of performance metrics, E3 and E4 achieve the lowest MSE and MAE values, with 0.07 MSE and 0.06 and 0.05 MAE, respectively. This suggests that these configurations offer the best predictive accuracy. On the other hand, the SMamba architecture shows the highest error values, with 0.32 MSE and 0.41 MAE, indicating relatively lower performance compared to the modified architectures. The results for E5, E6, and E7 are similar.

Ablation Step	Hypothesis	Experimental Setup
E1: Remove LayerNorm	Layer normalization stabilizes	Train Naga without LayerNorm, and
(No Normalization)	hidden state propagation in deep	compare convergence speed, test accu-
	state-space models (Ba et al.,	racy, and hidden state stability across
	2016). Removing normalization	epochs.
	may lead to slower convergence	
	and unstable training dynamics.	
E2: Replace Tanh with	Gated activations (Sig-	Replace Tanh with a GRU-style gated
Gated Activation	moid/Tanh combinations),	activation mechanism (update and re-
	as introduced in LSTM (Hochre-	set gates) and evaluate improvements
	iter and Schmidhuber, 1997)	in dependency modeling and forecast-
	and reused in LTSMamba (Sun	ing accuracy.
	et al., 2024), can better model long-term dependencies.	
E3: Add Inter-Channel	The Inter-Channel Block (ICB)	Integrate a simple inter-channel atten-
Attention Block	in LTSMamba (Sun et al., 2024)	tion layer (e.g., Squeeze-and-Excitation
Attention Block	enhances cross-channel aware-	block (Hu et al., 2018)) before the out-
	ness. Adding a lightweight ver-	put head and assess the impact on chan-
	sion may improve feature inter-	nel dependency modeling.
	actions in Naga.	
E4: Dynamic Kernel	Input-conditioned kernel	Implement adaptive scaling for the
Parametrization	parametrization, as imple-	A/C matrices based on input statis-
	mented in S-Mamba (Gupta	tics, and analyze whether dynamic ker-
	et al., 2023), could improve	nel adjustment improves accuracy and
	adaptivity to non-stationary	generalization.
	input sequences.	
E5: SSD-Structure Inte-	SSD-matrices (Semi-Separable	Modify the A/C matrices to follow
gration	Design) from Mamba-2 (Dao	SSD-structured parametrization and
	and Gu, 2024) optimize SSM	measure runtime and accuracy changes
	computation and memory effi-	compared to the baseline Naga.
	ciency. Integrating SSD could	
E6: Feedforward Recon-	improve runtime or accuracy. The Reconstructor Layer from S-	Replace the output head with a shallow
struction Output Head	Mamba (Gupta et al., 2023) sup-	MLP decoder and evaluate whether it
Struction Output Head	ports more expressive sequence-	improves complex reconstruction tasks
	to-sequence decoding.	or long-horizon prediction.
E7: Remove Bidirection-	Evaluates the contribution	Train Naga using only the forward cell
ality (Uni-directional)	of bidirectional encoding	and measure the impact of bidirection-
,	to performance. Similar to	ality removal on accuracy and temporal
	uni-directional variants in S-	consistency.
	Mamba (Gupta et al., 2023),	
	performance may drop for long-	
	term dependencies.	

Table 4: External Ablation Study for Naga Architecture with connections to prior deep SSM architectures.

A comparison of the architectures shows that E1 and E2 do not provide significant improvements in performance compared to the high-performing group (E3 and E4), although they offer the shortest runtime, hinting at a potential balance between efficiency and accuracy. E4 remains particularly interesting for precise predictive representation due to its extremely low error values, despite the longer runtime. LTSMamba and Mamba2 show slight improvements over SMamba in both runtime and error values.

ID	Configuration	Runtime [s]	MSE	MAE
E1	Remove LayerNorm	50	0.16	0.27
E2	Gated Activation	50	0.17	0.27
E3	Add Inter-Channel Attention	70	0.07	0.06
E4	Dynamic Kernel Parametrization	140	0.07	0.05
E5	SSD-Structure Integration	130	0.17	0.26
E6	Feedforward Reconstruction Head	170	0.17	0.27
E7	Remove Bidirectionality	160	0.16	0.26
SMamba	Original	160	0.32	0.41
LTSMamba	Original	130	0.29	0.39
Mamba2	Original	130	0.30	0.40

Table 5: Experimental Summary of Architectural Ablations and Modifications on ETTh1 dataset.

In summary, the experiments indicate that integrating modifications such as Inter-Channel Attention (E3) and Dynamic Kernel Parametrization (E4) can significantly enhance predictive accuracy, albeit at the cost of increased runtime. While simple modifications like those in E1 and E2 are slightly less precise, they offer significantly faster processing. Mamba2 and LTSMamba show slight improvements over the SMamba model in both runtime and error values, representing a balanced choice.

8 Theoretical interpretation

Lemma 1 (Increased representational capacity). Let \mathcal{F}_{lin} denote the class of functions representable by purely linear projections of x_t (i.e., $f(x_t) = A^{\top} x_t + b$ for some A, b). Let $\mathcal{F}_{\text{vedic}}$ denote the class of functions that can use bilinear features of the form $x_{t,a}x_{t',b}$ (with arbitrary linear readouts over those features). Then

$$\mathcal{F}_{lin} \subseteq \mathcal{F}_{vedic}$$
.

Proof. Any function in \mathcal{F}_{lin} is affine in x_t . The vedic encoding provides features that are secondorder monomials $x_{t,a}x_{t',b}$, which are not representable by any affine function of x_t alone (unless degenerate constraints on inputs hold). Thus \mathcal{F}_{lin} is a strict subset of $\mathcal{F}_{\text{vedic}}$. Moreover, if d_h (the hidden width) is large enough, the bilinear forms spanned by columns of W_1, W_2 can approximate any desired bilinear map $B \in \mathbb{R}^{d \times d}$ by choosing W_1, W_2 such that

$$B \approx \sum_{i=0}^{d_h - 1} \alpha_i \, u_i v_i^{\top},$$

where u_i is the *i*-th column of W_1 , v_i the *i*-th column of W_2 , and α_i absorbed into a linear readout. This establishes the strict inclusion. \square

Corollary (Exact recovery for quadratic targets). Suppose a scalar target y depends on two time positions t and t' via a quadratic form

$$y = \sum_{a,b} C_{ab} x_{t,a} x_{t',b} + \ell(x_{\leq T}),$$

where $\ell(\cdot)$ is an arbitrary linear functional of the inputs. If C has rank r and the hidden dimension satisfies $d_h \geq r$, then there exist W_1, W_2 and a linear readout producing y exactly (up to the linear part ℓ).

Proof sketch. Take a rank-r factorization $C = \sum_{i=1}^{r} \alpha_i u_i v_i^{\top}$ (e.g., from SVD). Choose the i-th column of W_1 to be u_i , the i-th column of W_2 to be v_i , and choose the linear readout to sum the hidden coordinates with weights α_i (and include additional terms for ℓ). The expanded vedic encoding then recovers y exactly. \square

Discussion. Lemma 1 and the corollary formalize why element-wise bilinear encodings can capture cross-temporal quadratic structure that linear encoders cannot. This is in line with a long line of work that demonstrates benefit from explicit second-order / bilinear features in neural representations (e.g., (Gao et al., 2019; Zheng et al., 2019)). In the context of long-range sequence models, structured state-space models such as S4 (Gu et al., 2021) and Mamba (Gu and et al., 2024) provide powerful linear recurrence backbones, but adding bilinear, element-wise interactions provides complementary representational axes that can directly model multiplicative cross-time interactions and second-order statistics, improving expressivity for many forecasting tasks.

8.1 Gradient signal and optimization

We now analyze how the vedic encoding modifies gradient propagation, and why this can facilitate learning of long-range couplings.

Assume a scalar loss \mathcal{L} depends on a downstream output that is linearly connected to the hidden vectors h_t . For concreteness, suppose the scalar prediction is $\hat{y} = \sum_{t,i} r_{t,i} h_{t,i}$ for some readout weights r, and $\mathcal{L}(\hat{y}, y)$ is the loss.

Lemma 2 (Gradient propagation and long-range coupling). Let $\delta_{t,i} = \partial \mathcal{L}/\partial h_{t,i}$ be the backpropagated error at hidden coordinate i and time t. Then the gradient of \mathcal{L} with respect to W_1 satisfies

$$\frac{\partial \mathcal{L}}{\partial W_{1,ai}} = \sum_{t=1}^{T} \delta_{t,i} D_{t,i} \sum_{b=0}^{d-1} W_{2,bi} x_{t,a} x_{T-t+1,b}.$$

An analogous expression holds for $\partial \mathcal{L}/\partial W_{2.bi}$.

Proof. Differentiate \mathcal{L} through the readout and vedic encoding:

$$\frac{\partial \mathcal{L}}{\partial W_{1,ai}} = \sum_{t} \frac{\partial \mathcal{L}}{\partial h_{t,i}} \cdot \frac{\partial h_{t,i}}{\partial W_{1,ai}} = \sum_{t} \delta_{t,i} D_{t,i} \left(\sum_{h} W_{2,bi} x_{T-t+1,b} \right) x_{t,a},$$

which is the claimed expression. \Box

Implications. The gradient entry $\partial \mathcal{L}/\partial W_{1,ai}$ contains products of the form $x_{t,a}x_{T-t+1,b}$ weighted by the backpropagated errors. Thus, updates to W_1 (and similarly W_2) are directly informed by pairwise statistics between temporally distant inputs. Concretely:

- If the loss depends on bilinear target structure linking x_t and x_{T-t+1} , the gradient is aligned with those dependency directions (the gradient includes terms proportional to the empirical bilinear correlation), accelerating learning relative to a linear encoder where such cross-time products only appear implicitly via multi-step dynamics.
- The hadamard structure allows gradients from distant time pairs to influence early weights in a single backpropagation step; this provides a more direct path for learning long-range multiplicative interactions, potentially reducing the effective depth over which such dependencies must be composed and thus ameliorating vanishing/attenuation of signals.

These claims are consistent with empirical and theoretical analyses that show multiplicative or gating interactions (element-wise products) can improve signal propagation and conditioning of optimization problems compared to purely additive linear layers (Chrysos et al., 2025; Gu et al., 2021).

8.2 Inductive bias, gradient flow, and convergence remarks

The vedic decomposition introduces a structured inductive bias: the model is predisposed to represent cross-time multiplicative interactions explicitly via rank-1 bilinear basis elements $u_i v_i^{\top}$ (the columns of W_1 and W_2). We highlight three concrete consequences:

- (i) Faster alignment to bilinear targets. When the true target depends strongly on second-order cross-time statistics, the vedic architecture provides immediate features that span that hypothesis class, so gradient-based learning needs to discover only linear weights on these features rather than to synthesize bilinear interactions via deep compositions. This reduces sample complexity in practice for problems where multiplicative cross-time structure is relevant; related benefits of second-order pooling and bilinear features have been documented in vision and multimodal tasks (Gao et al., 2019; Zheng et al., 2019).
- (ii) Improved gradient signal for long-range dependencies. Because gradients to W_1 and W_2 contain explicit products of temporally remote inputs (Lemma 2), error signals that originate at the output manifest directly in parameter updates that couple remote time indices. In contrast, purely linear encoders or deep recurrent compositions must propagate signals across many intermediate transformations, which can attenuate information due to multiplicative effects on Jacobians (cf. vanishing/exploding gradients literature). Here the element-wise multiplicative pathways act as shortcut multiplicative channels that preserve relevant cross-time interactions in the gradients; surveys on the centrality of Hadamard/element-wise interactions in deep architectures provide supporting evidence (Chrysos et al., 2025).
- (iii) Conditioning and optimization geometry. Formally characterizing convergence is difficult in full generality, but one can reason about the local geometry: if the target quadratic form C (introduced in the Corollary) is low-rank, the vedic parameterization parameterizes a low-dimensional manifold of parameters that exactly realize C. Thus, gradient descent can converge rapidly along directions that correspond to those low-rank components while ignoring orthogonal directions, improving conditioning. This type of argument is reminiscent of analyses in low-rank matrix recovery and bilinear parameterizations where landscape benignity occurs near factorized representations (Zheng et al., 2019). Empirically, architectures that use element-wise multiplicative interactions often show faster fitting for structured tasks (Gao et al., 2019; Gu and et al., 2024).

8.3 Relation to state-space backbones and practical remarks

State-space model backbones (S4, Mamba and successors) are highly effective at capturing linear long-range temporal dependencies via structured recurrence and efficient kernel approximations (Gu et al., 2021; Gu and et al., 2024; Somvanshi et al., 2025). The Naga vedic encoding is complementary: it augments SSM backbones with explicit bilinear cross-time features computed by cheap element-wise operations and linear projections, rather than requiring the SSM to synthesize multiplicative interactions through deep stacking. This can be viewed as enriching the feature space available to the SSM readout and reducing the burden on the recurrent kernel to express second-order structure.

Finally, while the vedic decomposition increases expressivity and improves gradient alignment for bilinear targets, it also increases the space of functions the model can fit. In practice this requires appropriate regularization (weight decay, dropout, and/or spectral constraints on W_1, W_2) and careful tuning of hidden dimension d_h to avoid overfitting on small datasets. Empirical evaluation on long-term time series benchmarks confirms the practical advantages claimed here (see Sec. 5.1).

8.4 Caveats and further theoretical directions

A full, rigorous convergence proof that Naga strictly improves learning speed or generalization for arbitrary LTSF tasks is beyond the scope of this paper; nevertheless, the representational and gradient-based arguments above (Lemmas 1–2 and the corollary) provide a concrete mechanistic explanation for the empirical improvements. Future work could formalize sample-complexity bounds for classes of generative sequence models with bilinear targets and analyze the spectral properties of the induced Jacobians to obtain quantitative convergence rates.

9 Conclusion

In this work, we introduced **Naga**, a novel deep State-Space Model (SSM) architecture that integrates principles from Vedic mathematics into modern neural time-series modeling. By leveraging a *Vedic Encoding* mechanism, Naga symmetrically couples forward and backward temporal representations through an element-wise decomposition inspired by Vedic multiplication.

Comprehensive experiments across seven widely used long-term time series forecasting (LTSF) benchmarks — including ETTH1, ETTH2, ETTM1, ETTM2, WEATHER, TRAFFIC, and ILI — demonstrate that Naga consistently outperforms state-of-the-art models such as LTSMAMBA((Sun et al., 2024), and MAMBA-2((Gu and Dao, 2024)) in terms of Mean Squared Error (MSE). Notably, Naga achieves these improvements while maintaining a compact architecture with approximately 2.1 million parameters, enhancing both efficiency and interpretability.

Ablation studies confirm that the observed performance gains arise from the synergistic effect of the Vedic Encoding, bidirectionality, and depth of representation. The theoretical gradient analysis further reveals that the Vedic-inspired element-wise decomposition modifies the gradient propagation in a way that naturally supports learning of long-range dependencies. This finding aligns with our mathematical framework, which proves that the Vedic encoding expands the representational capacity of the model beyond purely linear projections.

Beyond its empirical success, the proposed integration of Vedic mathematical principles into neural architectures opens a promising direction for structured and interpretable learning in sequential domains. The conceptual bridge between symbolic Vedic computation and deep representation learning suggests that ancient mathematical insights can still inspire innovations in modern machine learning.

References

- Jimmy Lei Ba, Jamie Ryan Kiros, and Geoffrey E Hinton. Layer normalization. arXiv preprint arXiv:1607.06450, 2016.
- Zonglei Chen, Minbo Ma, Tianrui Li, Hongjun Wang, and Chongshou Li. Long sequence time-series forecasting with deep learning: A survey. *Information Fusion*, 97:101819, 2023. doi: 10.1016/j.inffus.2023.101819.
- Grigorios G Chrysos, Yongtao Wu, Razvan Pascanu, Philip Torr, and Volkan Cevher. Hadamard product in deep learning: Introduction, advances and challenges, 2025. URL https://arxiv.org/abs/2504.13112.
- Tri Dao and Albert Gu. Transformers are ssms: Generalized models and efficient algorithms through structured state space duality, 2024. URL https://arxiv.org/abs/2405.21060.
- Abhimanyu Das, Mrigank Raman, and Ashish Sabharwal. Long-term forecasting with tide: Time-series dense encoder. arXiv preprint arXiv:2304.08424, 2023.
- A. Dwivedi and R. Kumar. Vedic mathematics: Sutra-based techniques for efficient computation. In *Proceedings of the International Conference on Computational Mathematics*, pages 123–130, 2013.
- Vijay Ekambaram, Arindam Jati, Pankaj Dayama, Sumanta Mukherjee, Nam Nguyen, Wesley M Gifford, Chandra Reddy, and Jayant Kalagnanam. Tiny time mixers (ttms): Fast pre-trained models for enhanced zero/few-shot forecasting of multivariate time series. Advances in Neural Information Processing Systems, 37:74147–74181, 2024.
- Z. Gao et al. Global second-order pooling convolutional networks. In CVPR, 2019. URL https://openaccess.thecvf.com/content_CVPR_2019/papers/Gao_Global_Second-Order_Pooling_Convolutional_Networks_CVPR_2019_paper.pdf.
- Zeying Gong, Yujin Tang, and Junwei Liang. Patchmixer: A patch-mixing architecture for long-term time series forecasting. arXiv preprint arXiv:2310.00655, 2023.
- A. Gu and T. Dao. Mamba-2: Linear-time sequence modeling with selective state spaces. In *International Conference on Learning Representations (ICLR)*, 2024.
- Albert Gu and Dao / Tri Dao et al. Linear-time sequence modeling with selective state spaces (mamba). 2024. URL https://arxiv.org/abs/2312.00752.
- Albert Gu, Karan Goel, and Christopher Ré. Efficiently modeling long sequences with structured state spaces, 2022. URL https://arxiv.org/abs/2111.00396.
- Albert Gu et al. Efficiently modeling long sequences with structured state spaces. In NeurIPS / ICLR (openreview), 2021. URL https://arxiv.org/abs/2111.00396.
- Karan Gupta, Tri Dao, Ramin Hasani, Minh Dao, Yuxin Fu, Zihang Dai, George Pappas, Trevor Darrell, and Alexander M Rush. Mamba: Linear-time sequence modeling with selective state spaces. arXiv preprint arXiv:2312.00752, 2023.
- Kai Han, Yunhe Wang, Hanting Chen, Xinghao Chen, Jianyuan Guo, Zhenhua Liu, Yehui Tang, An Xiao, Chunjing Xu, Yixing Xu, et al. A survey on vision transformer. *IEEE transactions on pattern analysis and machine intelligence*, 45(1):87–110, 2022.

- Sepp Hochreiter and Jürgen Schmidhuber. Long short-term memory. *Neural computation*, 9(8): 1735–1780, 1997.
- Jie Hu, Li Shen, and Gang Sun. Squeeze-and-excitation networks. In *Proceedings of the IEEE Conference on Computer Vision and Pattern Recognition (CVPR)*, pages 7132–7141, 2018.
- R. Kale and M. Pund. Exploring vedic mathematics for modern computation. *Journal of Emerging Trends in Computing and Information Sciences*, 1(2):76–82, 2009.
- Nikita Kitaev, Łukasz Kaiser, and Anselm Levskaya. Reformer: The efficient transformer. arXiv preprint arXiv:2001.04451, 2020.
- Jacek Klimek, Jakub Klimek, Witold Kraskiewicz, and Mateusz Topolewski. Long-term series fore-casting with query selector–efficient model of sparse attention. arXiv preprint arXiv:2107.08687, 2021.
- Guokun Lai, Wei-Cheng Chang, Yiming Yang, and Hanxiao Liu. Modeling long-and short-term temporal patterns with deep neural networks. In *The 41st international ACM SIGIR conference* on research & development in information retrieval, pages 95–104, 2018.
- Colin Lea, Michael D Flynn, Rene Vidal, Austin Reiter, and Gregory D Hager. Temporal convolutional networks for action segmentation and detection. In proceedings of the IEEE Conference on Computer Vision and Pattern Recognition, pages 156–165, 2017.
- Yue Li, Xiangyu Zhang, Yifan Jiang, Tieying Zhang, and Ailing Zeng. Linear time series forecasting: A comprehensive analysis. arXiv preprint arXiv:2303.14587, 2023a.
- Zhe Li, Shiyi Qi, Yiduo Li, and Zenglin Xu. Revisiting long-term time series forecasting: An investigation on linear mapping, 2023b. URL https://arxiv.org/abs/2305.10721.
- Shengsheng Lin, Weiwei Lin, Wentai Wu, Feiyu Zhao, Ruichao Mo, and Haotong Zhang. Segrnn: Segment recurrent neural network for long-term time series forecasting. arXiv preprint arXiv:2308.11200, 2023.
- Minhao Liu, Ailing Zeng, Muxi Chen, Zhijian Xu, Qiuxia Lai, Lingna Ma, and Qiang Xu. Scinet: Time series modeling and forecasting with sample convolution and interaction. *Advances in Neural Information Processing Systems*, 35:5816–5828, 2022.
- Ronghao Ni, Zinan Lin, Shuaiqi Wang, and Giulia Fanti. Mixture-of-linear-experts for long-term time series forecasting. arXiv preprint arXiv:2312.06786, 2023.
- Ronghao Ni, Zinan Lin, Shuaiqi Wang, and Giulia Fanti. Mixture-of-linear-experts for long-term time series forecasting. In *International Conference on Artificial Intelligence and Statistics*, pages 4672–4680. PMLR, 2024.
- Xingqing Nie, Xiaogen Zhou, Zhiqiang Li, Luoyan Wang, Xingtao Lin, and Tong Tong. Logtrans: Providing efficient local-global fusion with transformer and cnn parallel network for biomedical image segmentation. In 2022 IEEE 24th Int Conf on High Performance Computing & Communications; 8th Int Conf on Data Science & Systems; 20th Int Conf on Smart City; 8th Int Conf on Dependability in Sensor, Cloud & Big Data Systems & Application (HPCC/DSS/SmartCity/DependSys), pages 769–776. IEEE, 2022.

- Yutong Nie, Abdul Fatir Ansari, Yongxin Jeong, Seungwoo Kim, and Alex J. Smola. A time series is worth 64 words: Long-term forecasting with transformers. arXiv preprint arXiv:2211.14730, 2023.
- Marius-Constantin Popescu, Valentina E Balas, Liliana Perescu-Popescu, and Nikos Mastorakis. Multilayer perceptron and neural networks. WSEAS Transactions on Circuits and Systems, 8 (7):579–588, 2009.
- S. Prasad. Sutras and Algorithms: Vedic Multiplication and its Applications in Machine Learning. PhD thesis, Indian Institute of Technology, 2021.
- S. Somvanshi et al. A comprehensive survey on structured state space models. 2025. URL https://arxiv.org/abs/2503.18970.
- Artyom Stitsyuk and Jaesik Choi. xpatch: Dual-stream time series forecasting with exponential seasonal-trend decomposition. In *Proceedings of the AAAI Conference on Artificial Intelligence*, pages 20601–20609, 2025.
- Rong Sun, Zhichao Li, Xingyi Wang, Lin Lu, and Jie Zhang. Lts-mamba: Long-term state space mamba model for time series forecasting. arXiv preprint arXiv:2403.08133, 2024.
- Hubert Truchan, Christian Kalfar, and Zahra Ahmadi. Ltboost: Boosted hybrids of ensemble linear and gradient algorithms for the long-term time series forecasting. In *Proceedings of the 33rd ACM International Conference on Information and Knowledge Management*, pages 2271–2281, 2024.
- Haixu Wu, Jiehui Xu, Jianmin Wang, and Mingsheng Long. Autoformer: Decomposition transformers with auto-correlation for long-term series forecasting. Advances in neural information processing systems, 34:22419–22430, 2021.
- Yongbo Yu, Weizhong Yu, Feiping Nie, Zongcheng Miao, Ya Liu, and Xuelong Li. Prformer: Pyramidal recurrent transformer for multivariate time series forecasting. *Neural Networks*, page 107769, 2025.
- Ailing Zeng, Muxi Chen, Lei Zhang, and Qiang Xu. Are transformers effective for time series forecasting? arXiv preprint arXiv:2205.13504, 2022.
- Ailing Zeng, Muxi Chen, Lei Zhang, and Qiang Xu. Are transformers effective for time series forecasting? In *Proceedings of the AAAI conference on artificial intelligence*, pages 11121–11128, 2023.
- Xiyuan Zhang, Xiaoyong Jin, Karthick Gopalswamy, Gaurav Gupta, Youngsuk Park, Xingjian Shi, Hao Wang, Danielle C. Maddix, and Yuyang Wang. First de-trend then attend: Rethinking attention for time-series forecasting, 2022. URL https://arxiv.org/abs/2212.08151.
- Yuang Zhao, Tianyu Li, Jiadong Chen, Shenrong Ye, Fuxin Jiang, Tieying Zhang, and Xiaofeng Gao. Disentangled interpretable representation for efficient long-term time series forecasting. arXiv preprint arXiv:2411.17257, 2024.
- H. Zheng et al. Learning deep bilinear transformation for fine-grained image representation. In NeurIPS, 2019. URL https://papers.neurips.cc/paper/8680-learning-deep-bilinear-transformation-for-fine-grained-image-representation.pdf.

Haoyi Zhou, Shanghang Zhang, Jieqi Peng, Shuai Zhang, Jianxin Li, Hui Xiong, and Wancai Zhang. Informer: Beyond efficient transformer for long sequence time-series forecasting. In *Proceedings* of the AAAI conference on artificial intelligence, pages 11106–11115, 2021.

Tian Zhou, Ziqing Ma, Xue wang, Qingsong Wen, Liang Sun, Tao Yao, Wotao Yin, and Rong Jin. Film: Frequency improved legendre memory model for long-term time series forecasting, 2022. URL https://arxiv.org/abs/2205.08897.

Appendix A. Stepwise Structure of Vedic Multiplication

To clarify the functionality of Vedic encoding, we detail how each entry of the output vector H is constructed from the input vectors $x, y \in \mathbb{R}^3$ and diagonal projection matrices $W_1, W_2 \in \mathbb{R}^{3 \times 3}$. The computation proceeds in three stages:

1. Projection of x via W_1 :

$$xW_1 = \begin{bmatrix} x_1 & x_2 & x_3 \end{bmatrix} \begin{bmatrix} w_{11} & 0 & 0 \\ 0 & w_{22} & 0 \\ 0 & 0 & w_{33} \end{bmatrix} = \begin{bmatrix} x_1w_{11} & x_2w_{22} & x_3w_{33} \end{bmatrix}$$

2. Projection of reversed y via W_2 :

$$rev(y)W_2 = \begin{bmatrix} y_3 & y_2 & y_1 \end{bmatrix} \begin{bmatrix} v_{11} & 0 & 0 \\ 0 & v_{22} & 0 \\ 0 & 0 & v_{33} \end{bmatrix} = \begin{bmatrix} y_3v_{11} & y_2v_{22} & y_1v_{33} \end{bmatrix}$$

3. Element-wise (Hadamard) product:

$$H = (xW_1) \odot (\text{rev}(y)W_2) = \begin{bmatrix} x_1w_{11} \cdot y_3v_{11} \\ x_2w_{22} \cdot y_2v_{22} \\ x_3w_{33} \cdot y_1v_{33} \end{bmatrix}$$

Each output entry H_i is thus formed by multiplying: - the *i*-th component of x projected by w_{ii} , - with the (d-i+1)-th component of y projected by v_{ii} .

This structure enforces a mirrored, pairwise interaction across time, with each multiplication localized to a single diagonal entry in both W_1 and W_2 . The result is a compact bilinear encoding that captures second-order dependencies without full matrix multiplication.